ACS Catalysis

pubs.acs.org/acscatalysis
Research Article

Photoinduced CO_2 Conversion under Arctic Conditions—The High Potential of Plasmon Chemistry under Low Temperature

Anna Zabelina, Jakub Dedek, Olga Guselnikova, Denis Zabelin, Andrii Trelin, Elena Miliutina, Zdenka Kolska, Jakub Siegel, Vaclav Svorcik, Jiri Vana, and Oleksiy Lyutakov*

Cite This: ACS Catal. 2023, 13, 3830−3840

ABSTRACT: The conversion of CO_2 to fine chemicals is an efficient tool for reducing the negative impact of human activities on the environment. In this work, we show that CO_2 capture and its sunlight-based activation can proceed efficiently even at low, practically arctic temperatures with the implementation of so-called plasmon-assisted chemistry. We propose the specific photocatalyst consisting of two parts: (i) an organic shell responsible for CO_2 capture and (ii) a plasmon-active metal nanoparticle core for activation of entrapped CO_2 and involving it in the cycloaddition reaction. The effect of temperature on the plasmon-assisted CO_2 cycloaddition was studied, and a reaction with only slight temperature sensitivity was observed. Theoretical calculations indicated a significant decrease in the "apparent" activation barrier of the reaction under the plasmon-assisted mechanism. Our results open an opportunity for the world economy to exploit the vast Arctic and Antarctic (or close to them) territories where the powerful solar potential is practically not used yet.

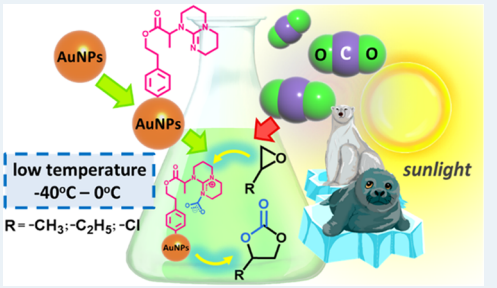

KEYWORDS: *photocatalysis, hybrid catalyst, plasmon-assisted chemistry, CO_2 cycloaddition, low temperature*

1. INTRODUCTION

Contemporary low-temperature chemistry provides unique information about the behavior of reactive substances at low temperatures and about the phenomena that occur when moving from "standard" temperatures to much lower ones.[1] To date, processes such as plasma catalysis, electrocatalysis, sonocatalysis, mechano-catalysis, and biocatalysis have been studied at low temperatures.[2,3] In addition, photocatalysis is a promising option to be realized at low reaction temperatures.[4] Activation of stable and common molecules such as methane, nitrogen, and carbon dioxide at low temperatures, i.e., close to arctic conditions, is essential from the point of view of future sustainable energy/chemical systems.[5,6] Moreover, according to recent reports,[7] the north territories are undergoing a rapid shift into a new warmer regime accompanied by permafrost melting and emission of greenhouse gases. Therefore, the possibility of CO_2 activation at low temperatures could not only improve the environmental conditions in these regions but also facilitate the use of CO_2 waste.

In general, CO_2 is a relatively inert molecule and its activation suffers from energy efficiency and poor reaction rates.[8−10] Thus, photocatalytic CO_2 activation using sunlight is very attractive due to the availability and zero cost of this energy source even in the North territories.[11−14] From photocatalysis studies performed at common temperatures, we learned different strategies for CO_2 activation, including the exploration of novel semiconductors with narrow band gaps and the development of specific catalytic surface sites.[15−17] The main idea here is to change the reaction pathways and decrease the "apparent" reaction activation barrier for CO_2 activation. This can be achieved photoelectrochemically through changes in the electronic or polarization states of the materials (both catalysts or reagents).[18,19] In the case of plasmon-assisted photochemistry, the light energy is used for plasmon excitation with a related appearance of hot charge carriers or high-energy states, which can be transferred to surrounding materials.[20,21] In most related works, the plasmon-assisted process accelerates the electrochemical reduction of CO_2, with the formation of various products, such as CO, CH_3OH, or CH_4.[22−25] For the transformation of CO_2 into fine organic products, the lowering of the apparent reaction activation barrier to close to zero level has also been reported, using plasmon excitation on the surface of noble-metal nanostructures.[26−30] As a result, plasmon-assisted chemical transformations can be performed at significantly lower temperatures, compared to traditional reaction routes.[31−35]

In this work, we investigate the plasmon-assisted CO_2 activation at temperatures significantly below zero, taking into account the fact that an increase in CO_2 concentration in

Received: November 30, 2022
Revised: February 8, 2023
Published: March 3, 2023

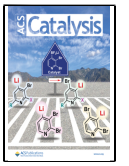

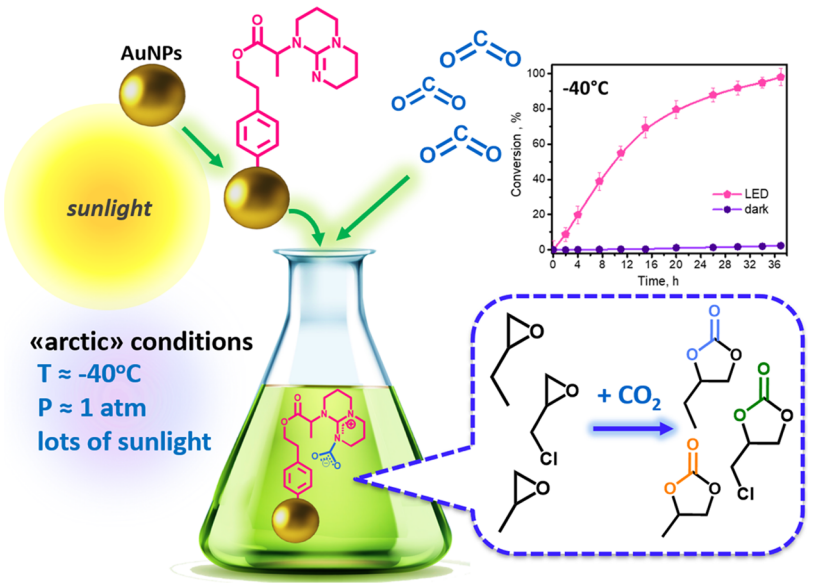

Figure 1. Schematic representation of the preparation of AuNPs-TBD hybrid catalysts for CO_2 cycloaddition to three different epoxides.

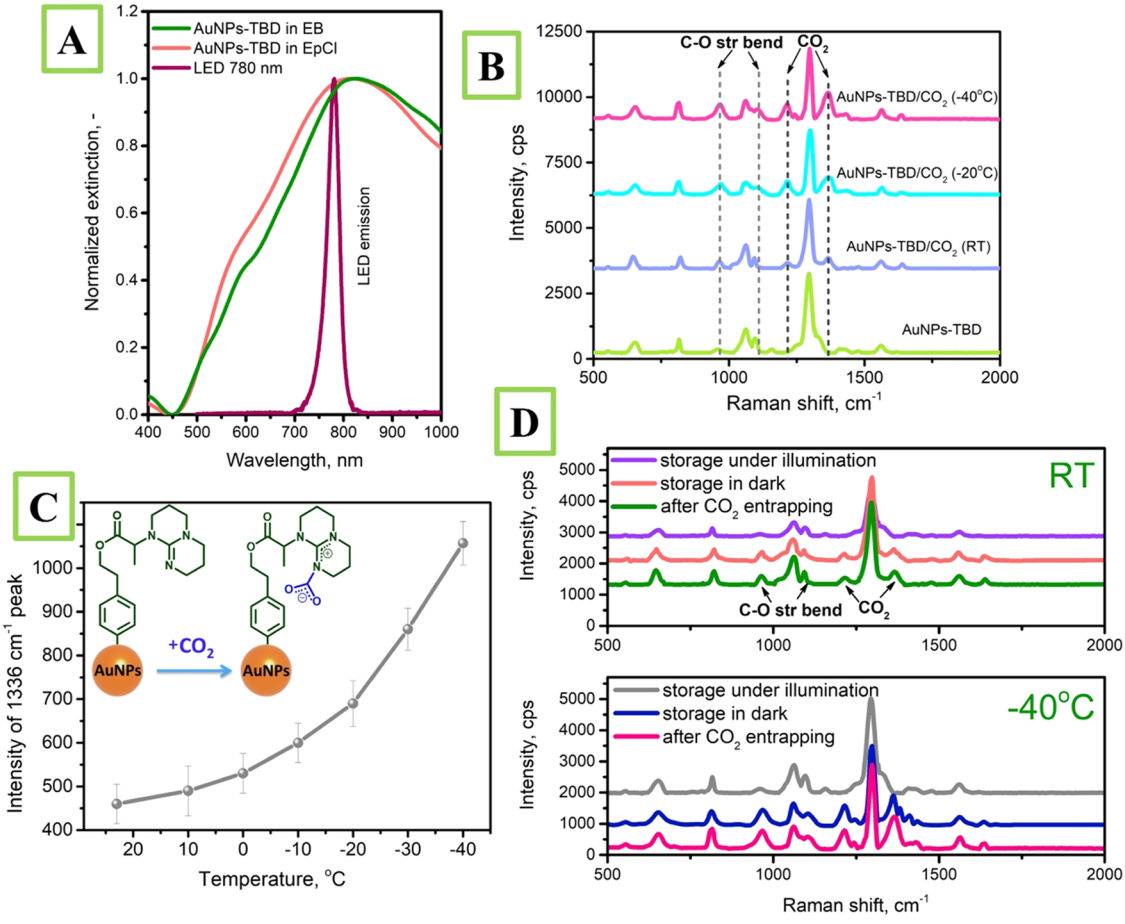

Figure 2. Conformation of CO_2 capture by AuNPs-TBD and its plasmon-assisted release: (A) UV−vis spectra of AuNPs-TBD suspension in three epoxides. (B) SERS spectra measured after AuNPs-TBD interaction with CO_2 in methanol at different temperatures (nanoparticles were sedimented from methanol and immediately subjected to measurements without change of temperature). (C) Dependency of characteristic CO_2 peak intensity on the temperature of creation of AuNPs-TBD/CO_2 zwitterionic adducts (methanol was used as solvent). (D) Stability of characteristic CO_2 peaks (i.e., zwitterionic adduct) storage in dark or under illumination at RT and −40 °C temperatures.

the reaction medium can be reached with a temperature decrease. The plasmon-assisted CO_2 activation at low temperatures allows the utilization of sole sunlight energy, which is important in some unusual places, e.g., Polar Regions or some regions of Europe or North America[36] where other energy sources are not available. Without a doubt, the

https://doi.org/10.1021/acscatal.2c05891
ACS Catal. 2023, 13, 3830−3840

development of CO_2 utilization technologies in these regions may seem somewhat strange at first glance. However, given both the global growth of the human population and the depletion of nonrenewable resources (a significant amount of which is located in the northern and polar territories), and the large average amount of sunlight in the polar territories (which is comparable with the amounts of sunlight energy in such territories as central Europe),[37−39] the proposed approach may be of future importance.

2. EXPERIMENTAL PART

The preparation of gold nanoparticles (AuNPs) and the decoration of AuNPs with 1,5,7-triazabicyclo [4.4.0] dec-5-ene chemical moieties (further designated as AuNPs-TBD) were carried out according to previously reported procedures.[35] Experimental details are described in the Supporting Information (SI).

2.1. General Procedure of Plasmon-Assisted CO_2 Cycloaddition. The CO_2 cycloaddition was carried out in a septum-sealed flask at different temperatures from room temperature (RT) to −40 °C. First, 3 mg of AuNPs-TBD was sonicated in 3 mL of epoxide with the addition of tetrabutylammonium bromide (TBAB). The reaction flask was then placed in a thermal chamber and filled with CO_2 at the desired temperature. The reaction mixture was illuminated with a light-emitting diode (LED, 780 nm, 25 mW/cm^2) under continuous purging with CO_2 from a regular 3 L balloon via the needle. After the reaction stopped, the AuNPs-TBD were separated by centrifugation and the supernatant was analyzed using gas chromatography (GS) and ^{1}H and ^{13}C nuclear magnetic resonance (NMR) techniques

3. RESULTS AND DISCUSSION

3.1. Main Proposed Concept and AuNPs-TBD Preparation. Hybrid plasmonic catalysts (combining plasmonic and catalytic functions) have great potential in CO_2 conversion and other relevant chemical transformations.[40,41] In our work, a hybrid plasmonic catalyst has been prepared according to a recently published report.[35] Briefly, the spherical AuNPs were modified to attach hydroxyl groups, which were further coupled with 2-bromopropionyl bromide, and finally, TBD was immobilized on the surface (Figure S1). The confirmation of the plasmonic catalyst structure and full characterization of AuNPs-TBD is present in the SI (Figures S2 and S3 and related discussion). It is well known that TBD spontaneously forms a stable and isolable zwitterionic complex with CO_2,[42] ensuring its efficient entrapment from the surrounding solution(s) near the active surface (Figure 1). After preparation, AuNPs-TBD nanoparticles were dispersed in epoxides and illuminated with wavelength, corresponding to plasmon excitation at various temperatures and continuous purging with CO_2 at atmospheric pressure. As mentioned above, the immobilization of CO_2 will proceed spontaneously, forming a stable TBD-CO_2 adduct. Plasmon excitation will provide the energy required for the activation of the TBD-CO_2 adduct and its subsequent reaction with epoxides with the formation of the corresponding carbonates (Figure 1). As a result, we expected this hybrid system to interact with CO_2-forming carbonates without the need for elevated CO_2 pressure and even at low temperatures.[31−34] To fully verify this assumption, we used different epoxides, which can be ordered as follows, according to the simplicity of their interaction with CO_2: 1,2-epoxybutane > epichlorohydrin > propylene oxide (further referred to as EB, EpCl, and PO, respectively) and estimated CO_2 cycloaddition (Figure 1).

Since CO_2 cycloaddition will be performed under solvent-free conditions in pure epoxides, we estimate the plasmon-related optical properties of AuNPs-TBD in organic solvents. The UV−vis spectra of the AuNPs-TBD suspension in epoxides are presented in Figure 2A, where an increase in the plasmon bandwidth and its pronounced redshift (compared to water) are evident (see also Figure S2). The shift of the plasmon absorption band cannot be attributed only to the changes in the surrounding refractive indexes, which is not large enough (1.385, 1.436, and 1.366 for EB, EpCl, and PO, respectively, vs 1.333 for water). The observed shift (as well as widening) of the plasmon absorption band peak can be explained both by the nanoparticles and/or by the appearance of the faster plasmon decay channel, as a result of the presence of TBD on the surface. A similar effect was previously observed on hybrid plasmonic systems.[43,44] The position of the plasmon absorption band in epoxides determines the wavelength(s) subsequently used light source. In fact, all further experiments were performed with 780 nm light, which overlaps well with the plasmon absorption band AuNPs-TBD in all three epoxides.

3.2. CO_2 Capturing by AuNPs-TBD. In the next step, we estimated the ability of CO_2 capture by TBD under normal pressure and at various temperatures. The freshly prepared AuNPs-TBD suspension in methanol was bubbled with CO_2 at different temperatures and then characterized by dynamic light scattering (DLS) or surface-enhanced Raman spectroscopy (SERS) measurements (SERS measurements were performed in solid state mode, immediately after nanoparticle sedimentation under constant temperature). According to DLS data, the increase in the hydrodynamic radius of AuNPs-TBD after CO_2 bubbling confirmed AuNPs-TBD/CO_2 formation (Figure S5). SERS spectra measured on Au-TBD before and after CO_2 entrapment at RT and −40 °C provide the spectroscopic conformation of the formation of the TBD/CO_2 zwitterionic complex. In particular, CO_2 entrapment leads to the spontaneous appearance of new characteristic SERS bands at 966, 1106, 1216, and 1336 cm^{-1} (Figure 2B). The intensity of these peaks correlates with the amount of entrapped CO_2. The CO_2-related peak at 1336 cm^{-1} was used to evaluate the amount of CO_2 entrapped at both temperatures. As can be seen from Figure 2C, the intensity at 1336 cm^{-1} increases with decreasing temperature. So, CO_2 capture and zwitterionic adduct formation proceed more efficiently at low temperatures, apparently due to an increase in CO_2 concentration in methanol.[45] A similar phenomenon can be expected in the solubility of the case of epoxides; the solubility of CO_2 in epoxides is shown in Figure S6. So, at lower temperatures, more CO_2 molecules will be dissolved in organic solvents and subsequently entrapped by AuNPs-TBD, where they are available for further plasmonic triggering.

3.3. Plasmon-Assisted CO_2 Cycloaddition. After checking that the plasmon assistance can activate the created TBD-CO_2 zwitterionic adduct, we proceed to the utilization of AuNPs-TBD hybrid catalyst for plasmon-assisted CO_2 cycloaddition. In contrast to the previous experiments, we used different light wavelengths to activate the CO_2 adduct, which corresponds to the peak of the plasmon resonance of AuNPs-TBD-CO_2 in organic solvents. Of course, the use of different wavelengths may lead to the excitation of charge carriers with

https://doi.org/10.1021/acscatal.2c05891
ACS Catal. 2023, 13, 3830−3840

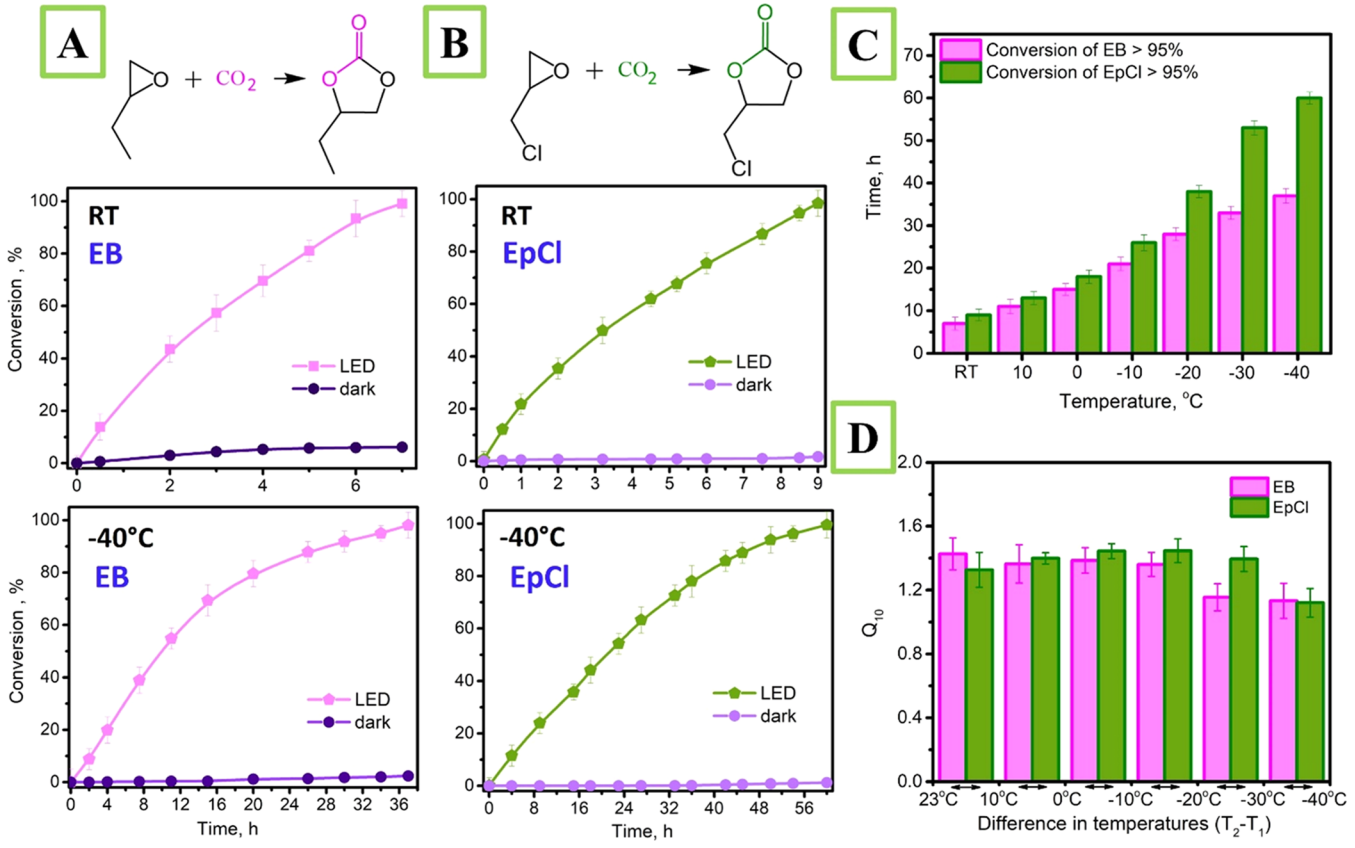

Figure 3. Conversion of epoxides at different temperatures under plasmon triggering or in dark: (A) EB, (B) EpCl; (C) time required for conversion of epoxides (above 95%) as a function of surrounding temperature; (D) calculated values of Q_{10} for two epoxides as a function of temperature range.

different energies. On the other hand, we assumed that in this case, plasmon triggering will also lead to the activation of the CO_2 adduct. The plasmon-assisted activation of AuNPs-TBD adduct with CO_2 was studied at RT and −40 °C (after separation and storage in the dark or under light illumination). At both temperatures and during storage in the dark, we observed the conservation of the characteristic peaks of the entrapped CO_2 (Figure 2D), indicating that there is no spontaneous CO_2 release. However, the illumination (595 nm wavelength was chosen according to UV−vis data in Figure S7) of AuNPs-TBD/CO_2 with plasmon triggering led to the disappearance of characteristic CO_2 bands, independently of the temperature. So, the as-created zwitterionic adduct is stable and can be activated by plasmon triggering. Plasmon triggering leads to the release of a CO_2 molecule(s) or their participation in chemical transformation (according to our assumption and preliminary results[35]).

After verifying that plasmon assistance can activate the TBD-CO_2 zwitterionic adduct, we proceed to the use of AuNPs-TBD hybrid catalyst for plasmon-assisted CO_2 cycloaddition. We used three different epoxides and performed cycloaddition at RT and at −40 °C, also taking into account the higher solubility of CO_2 at lower temperatures (Figure S6). The formation of all reaction products and reaction proceedings were monitored using GS and NMR methods (Figures S8−S14).

The time-resolved conversion of epoxides is presented in Figure 3A−D (and Figures S15 and S16) for two temperatures, RT and lower (−40 °C), while Table 1 shows the reaction yields. All experiments were carried out in the dark or under illumination. All epoxides besides EB do not spontaneously react with CO_2, but the reactions proceed successfully under plasmon triggering. The epoxides conversion and carbonates yield are in accordance with the reactivity of epoxides, ordered as follows: EB > EpCl > PO. The reaction rate at −40 °C and under plasmon triggering slowed 4−6 times compared to that at RT (Figure 3A−C). Despite the deceleration of the cycloaddition observed for all three epoxides, the reaction(s) still proceed efficiently even at very low temperatures (close to arctic conditions). In the next step, we analyzed the deceleration taking into account the common van't Hoff law. The temperature decrease by ca. 60 °C (from +23 to −40 °C) should lead to the reaction deceleration by a factor of (2−4)[6] (i.e., 60−4000 times), but only a decrease of ca. 3−6 times was observed.

To highlight this fact, we present the Q_{10} coefficient calculated according to $Q_{10} = \left(\frac{R_{T2}}{R_{T1}}\right)^{10/(T_2-T_1)}$, where R's are the reaction rates and T are the reaction temperatures. This coefficient gives the deceleration of a chemical process when the reaction mixture is cooled by 10 °C as a function of the temperature intervals (Figure 3E and Figure S15). For the Q_{10} evaluation, we used the moments when the quantitative yield (above 95%) of carbonates is achieved (except for the PO case, where the time for the 55% conversion was used). Generally, for chemical transformations, the Q_{10} coefficient usually lies in the range of 2−4. In the case of plasmon-assisted CO_2 cycloaddition to EB, we obtained significantly lower values of Q_{10} for all temperature ranges. In the case of EpCl, the Q_{10}

https://doi.org/10.1021/acscatal.2c05891
ACS Catal. 2023, 13, 3830−3840

Table 1. Plasmon-Assisted Reaction Parameters and Corresponding Yield(s)

temperature (°C)	time (h)	light	conversion[a] (%)	yield[a] (%)
		1,2-Epoxybutane		
RT	7	ON	99	95
		OFF	6	4
10	11	ON	98	94
		OFF	5	3
0	15	ON	98	96
		OFF	4	3
−10	21	ON	99	94
		OFF	4	3
−20	28	ON	97	95
		OFF	3	2
−30	33	ON	99	96
		OFF	2	1
−40	37	ON	98	96
		OFF	<2	<1
		Epichlorohydrin		
RT	9	ON	98	96
		OFF	<2	5
10	13	ON	98	95
		OFF	<2	<2
0	18	ON	97	93
		OFF	<1	<1
−10	26	ON	97	92
		OFF	<1	<1
−20	38	ON	98	95
		OFF	<1	<1
−30	53	ON	98	95
		OFF	<1	<1
−40	60	ON	99	97
		OFF	<1	<1

[a]Yield and conversion were defined by GC as incorporation of Au-TBD-CO_2 into cyclic carbonates. Reaction conditions: 2.5 mL of epoxide, CO_2 (1 atm), Au-TBD (3 mg), TBAB (0.8 mol %), solvent-free.

values were also lower compared to common cases. Finally, for PO, the Q_{10} was close to the normal value of 2 but decreased at temperatures below 0 °C. So, the main conclusion is that plasmon triggering significantly decreases the sensitivity of CO_2 cycloaddition to temperature decrease. This observation can be explained by two phenomena: (i) increase in CO_2 solubility in organic solvents and (ii) changes or reaction pathway (with a decrease of the apparent thermodynamic barrier) under plasmon triggering. However, the temperature dependence of Q_{10} indicates the impact of CO_2 solubility (Figure S6), which was increased only by a factor of 5−10 in the temperature range of RT to −40 °C. Thus, only increased solubility cannot fully explain the independence of the reaction rate on temperature.

3.4. Control Experiments. To reveal the contribution of plasmon excitation to low-temperature CO_2 cycloaddition, we performed a few control experiments, accomplished without catalysts or illumination. The results of these experiments, performed at RT and −40 °C (Figure S17), indicate that the illumination switching off or the removal of the catalyst interrupted the reaction. Similarly, in the absence of TBD grafting on the AuNP surface (i.e., the addition to the reaction mixture with dispersed AuNPs of an equal amount of not grafted TBD), the reaction did not proceed either (Figure S18). We also tested AuNPs without TBD (Figure S18) or with the addition of TBD without AuNPs (Figure S19). These experiments were performed under illumination at −40 °C, and we did not observe any EB conversion. Thus, the plasmon assistance and CO_2 entrapment near the plasmon-active substrate are necessary conditions for successful reaction proceeding.

In addition to the importance of the hybrid catalyst structure, we also studied the possible effects of plasmonic heating. First, monitoring the temperature of the reaction mixture under illumination indicated a negligible increase in the "reaction volume" temperature (Figure S20). We also performed the addition of CO_2 (also at RT and lower temperature) under illumination with different light powers or apertures, according to the experimental route described in a recently published article.[46] A linear dependence would indicate a photochemical process, whereas an exponential increase would rather be the signature of a photothermal effect. Figure S21 indicates the perfect linear dependence of EB conversion on the applied light power, which is a signature of the absence of photothermal effects. In the case of aperture radius variation (Figure S22), we observed a deviation from the expected quadratic dependence (characteristic for plasmon catalysis without the participation of plasmon heating). Probably, in this case, the previously predicted effect of heat dissipation occurs (the proposed "ideal" quadratic dependence assumes heat diffusion in an infinite surrounding medium and some deviation from the ideal behavior can be observed due to the different local thermal conductivity in the surrounding medium where the reaction proceeds).[46] An observed negligible impact of plasmon heating could be expected since constant illumination of spherical AuNP (with moderate light intensity) cannot produce significant heating, even when close to the nanoparticle surface space (unlike the case of nano- or femto-pulsed laser utilization).

As an additional argument, often used in favor of plasmon heating, namely, the agglomeration of NPs can lead to spatial "proximity" of several heating sources and a more pronounced increase in temperature. In our case, despite the fact that we did not observe obvious agglomeration of nanoparticles with the formation of large agglomerates (microscopic photos are shown in Figure S23), the results of DLS show that some agglomeration still occurred. To assess the potential impact of this phenomenon on plasmon heating, we performed a series of calculations (described in SI Figure S24). As expected, agglomeration of nanoparticles leads to some increase in temperature at the "hottest" point of the agglomerate. However, this increase was far from significant enough to affect the mechanism of plasmon catalysis.

Taking into account the preliminary exclusion of plasmon heating, as well as two alternative mechanisms of plasmon catalysis (direct or indirect energy or charge transfer), we performed a series of additional experiments to study the wavelength dependence of reaction efficiency (Figure S25). As can be seen, the reaction conversion does not correlate completely with the absorption profile of the plasmon-active catalyst. Therefore, based on previously reported work, we can assume that plasmonic photocatalysis occurs by the direct charge transfer mechanism without the injection of hot electrons and through the plasmon-induced excitation of the inner electron in the TBD-CO_2 adduct.[44,47−49]

3.5. DFT Calculations of Plasmon-Assisted CO_2 Cycloaddition. Photochemical plasmon catalysis is com-

https://doi.org/10.1021/acscatal.2c05891
ACS Catal. 2023, 13, 3830−3840

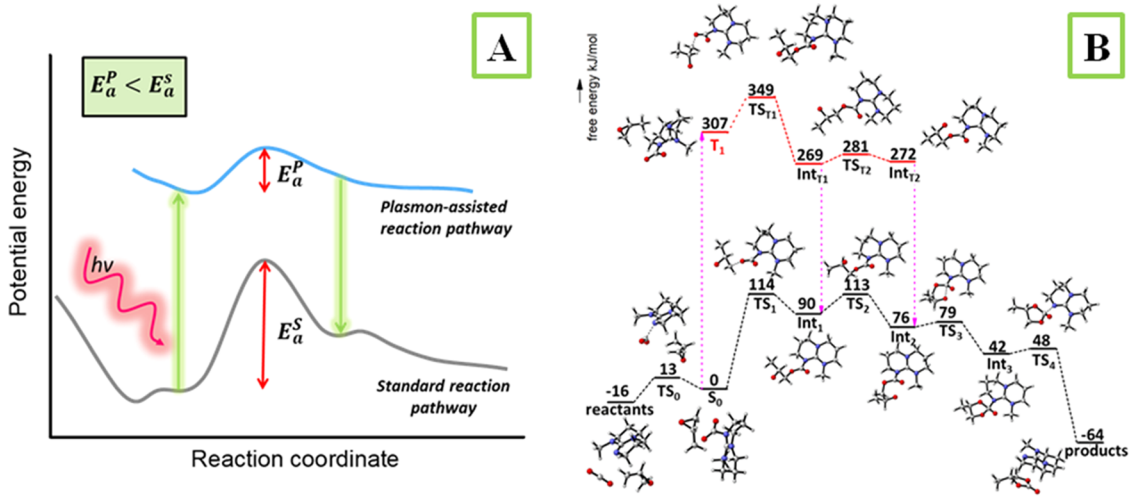

Figure 4. (A) Schematic representation of the reduction of apparent (i.e., residual) thermodynamic barrier in plasmon-assisted CO_2 cycloaddition; (B) comparison of reaction profiles for ground state (black) and triplet (red) reaction pathways calculated at the B3LYP/6-311+G** level of theory using dispersion correction GD3BJ and CPCM (diethylether) solvent model.

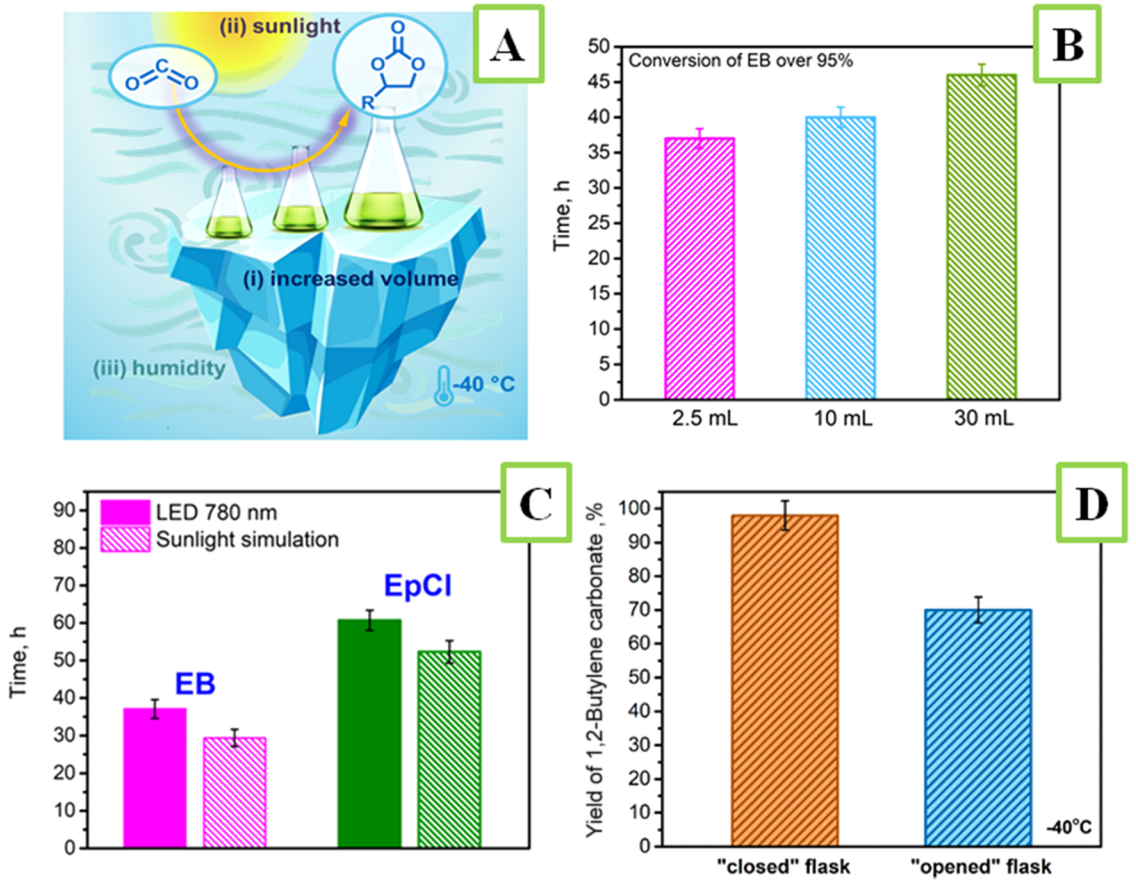

Figure 5. Demonstration of the technological attractiveness of the proposed approach: (A) approximated Arctic conditions (low temperature, availability of sunlight, and low absolute humidity); (B) reaction scalability: time required for plasmon-assisted EB conversion to 1,2-butylene carbonate over 95% at −40 °C as a function of a reaction volume; (C) comparison of experiments using LED and sunlight simulator: time periods required for plasmon-assisted conversion of EB and EpCl > 95% at −40 °C; (D) comparison of 1,2-butylene carbonate yield achieved after 37 h of plasmon-assisted cycloaddition at −40 °C (i.e., with or without the presence of residual moisture in the surrounding) reached in "opened" and "closed" flask.

monly attributed to the intramolecular excitation or injection of hot electrons from a metal surface to organic species. In both cases, the appearance of an alternative reaction pathway and the reduction of the apparent thermodynamic barrier can be expected, as is schematically depicted in Figure 4A. To verify the potential reaction mechanism, we performed density functional theory (DFT) (S5) calculations in a simplified model with the involvement of *N*-methylated TBD as the

https://doi.org/10.1021/acscatal.2c05891
ACS Catal. 2023, 13, 3830−3840

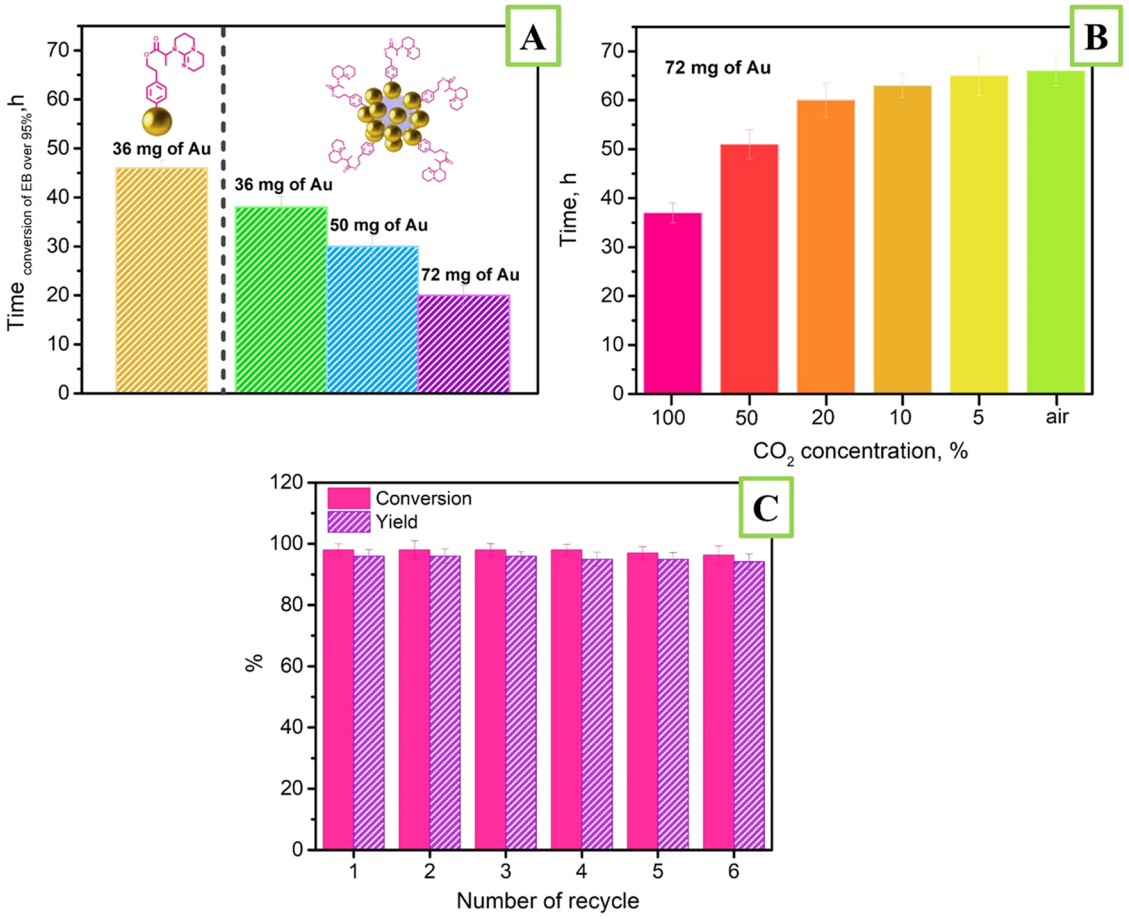

Figure 6. Time periods required for plasmon-assisted conversion of EB >95% at −40 °C: (A) as a function of increased amounts of AuNPs-TBD (utilization of Al_2O_3@AuNPs-TBD instead of AuNPs-TBD) or (B) dilution of used CO_2 gas by nitrogen as well as utilization of air as CO_2 source (reaction volume, 30 mL (utilization of Al_2O_3@AuNPs-TBD instead of AuNPs-TBD)); (C) several cycles of re-utilization of Al_2O_3@AuNPs-TBD in CO_2 cycloaddition to EB.

model substrate. In this case, methyl imitates the properties of the linker and at the same time prevents the involvement of the second nitrogen atom during the fixation of epoxides.[50] The energy profile (Figure 4B) for the ground state reaction pathway shows that the fixation of CO_2 is only slightly endergonic with the energy barrier of TS_0 29 kJ/mol. The rate-limiting step (114 kJ/mol) is the attack of one oxygen from CO_2 on the oxirane ring connected with its opening (TS_1). This is followed by rotation (TS_2) and closure of the carbonate ring (TS_3). In the last stage, the product is released (TS_4) and the catalyst enters the new catalytic cycle. As we have recently shown,[26,34] the plasmon-assisted [3 + 2] cycloaddition can occur via the triplet pathway (REF). In our case (Figure 4B), the triplet state of the complex of TBD-CO_2 with epoxide (T_1) is 307 kJ/mol, i.e., it is higher compared to that of the analogous ground state S_0. More importantly, the energy of TS_{T1} is only 45 kJ/mol above T_1. It should also be noted that TS_{T1} is not a complete analogue of TS_1. In this case, the oxirane ring is opened more easily. This indicates a possible energy transfer from TBD-CO_2 to epoxide prior to oxygen attack. As result, the activation energy is almost 3 times lower compared to that of the ground-state pathway, which is consistent with our experimental results. All attempts to find TS for ring closure failed, and the energies of triplet structures analogous to Int_3 and TS_4 are too high. This confirms the fact that ring closure and product release occur after loss of excitation and return to the ground-state reaction pathway. As an experimental verification of the calculated plasmon-assisted reaction pathway with participation of the triplet state, we performed several additional experiments using COT as the scavenger of exited states. The results presented in Figure S26 show that the addition of COT apparently quenches the reaction, which observation perfectly correlates with the performed DFT calculations.

3.6. Technological Attractiveness Demonstration. In the last part of the work, we demonstrated the technological attractiveness of the proposed approach by: (i) increasing the volume of the reaction mixture, (ii) utilizing sunlight instead of a single-wavelength LED (at −40 °C), and (iii) increasing the humidity in the reaction "surrounding". These additional experiments were carried out taking into account the "Arctic" conditions—low temperature, sufficient sunlight flux, and low absolute humidity (Figure 5A). First, the scalability tests (Figure 5B) indicate some decrease in the reaction efficiency with volume increase (under the conservation of catalyst/volume ratio). Such a phenomenon can be attributed to insufficient mixing of AuNPs-TBD nanoparticles under mechanically induced stirring or gradual decrease of the light intensity with its penetration into a larger volume of the reaction medium. We also compare the results of LED illumination with simulated sunlight triggering using a solar simulator (the power on the sample surface was adjusted to be

https://doi.org/10.1021/acscatal.2c05891
ACS Catal. 2023, 13, 3830−3840

100 mW/cm^2). According to the time required for the conversion of epoxides, the CO_2 cycloaddition is slightly decelerated with the utilization of sunlight simulator, the deceleration being less than 25% for all epoxides (Figure 5C) was observed.

Generally, the fact that CO_2 cycloaddition is sensitive to moisture due to possible hydrolysis[35] significantly complicates its technological implementation. However, a decrease in the reaction temperature to extremely low values leads to the suppression of humidity in the air (Figure S27). Thus, it is possible to avoid technical difficulties associated with the presence of moisture using plasmon-assisted CO_2 cycloaddition at −40 °C. To assess this possibility, we performed CO_2 cycloaddition in an opened flask (the reaction chamber was preliminarily saturated with water vapor at RT and then cooled to −40 °C). The results showed that the amount of obtained 1,2-butylene carbonate decreased only by 30% compared to the case of the septum-sealed flask (Figure 5D). We also evaluated the possibility of using low concentrations of CO_2 down to the atmospheric concentration (Figure S28). The results obtained show that a decrease in the concentration of CO_2 led to a rather significant slowdown of the reaction rate, observed in both cases, at RT and lower temperatures. However, at low temperatures, the observed decrease in the reaction rate was not as significant as in the RT case. This phenomenon can be explained by better solubility at low temperatures. In the case of low temperatures, we could use only air without its preliminary drying, which was not possible in the case of room temperature.

As already was shown, we observed a slowdown in the reaction rate both with an increase in the volume of the reaction mixture and a decrease in the CO_2 concentration in the initial mixture of gases. To compensate for these shortcomings, we tried immobilization of AuNP-TBD on the surface of Al_2O_3 microparticles. This approach allowed us to introduce a larger amount of AuNPs-TBD in the reaction mixture (in contrast to nonimmobilized AuNPs, which tend to agglomerate when a certain critical concentration is reached). The utilization of immobilized nanoparticles also allowed us to avoid plasmon heating, which is usually associated with nanoparticle aggregation.

The preparation and characterization of Al_2O_3@AuNPs-TBD are presented in the SI (Figures S29 and S30), while the "opened" reactor design is shown in Figure S31. Interestingly, even in the case of immobilized nanoparticles that cannot physically agglomerate, we observed an expansion of the plasmon peak, which correlates with the assumption of the presence of a faster plasmon decay channel due to the presence of TBD (Figure S32). The conversion of EB using this catalyst is shown in Figure 6, where special attention is paid to compensating for the negative effect of low temperature and the increase in reaction volume (Figure 6A). Furthermore, the utilization of Al_2O_3@AuNPs-TBD allowed us to significantly accelerate the reaction rate in the case of a large volume of reaction mixture and a lower CO_2 concentration (up to the use of air as a CO_2 source) as is shown in Figure 6B. An additional advantage of this approach is the fact that we can use air without pre-drying, which is impossible at room temperature due to the presence of natural humidity (Figure S31). Of course, in this case, the necessary amount of gold increases, but this fact is easily compensated by very simple removal of the catalyst and its re-utilization in several subsequent cycles without loss of catalyst efficiency (Figure 6C). Thus, taking into account the results of experiments carried out in "closer" to realistic conditions, as well as the availability of solar energy in the polar regions (which are already beginning to be used), we can talk about a fairly large potential for plasmonic chemistry (in particular, in application to CO_2 conversion for useful products) under the conditions of the polar regions (or regions close to them).

As a final remark, it should be noted that we demonstrated the plasmon-assisted CO_2 activation at temperatures significantly below zero, taking into account the fact that an increase of CO_2 concentration in the reaction medium can be reached with temperature lowering. Plasmon-assisted CO_2 activation at low temperatures allows the utilization of sole sunlight energy, which could be important in some unusual places (e.g., Polar Regions), where other energy sources are not available. Without a doubt, the use of solar energy in the Polar Regions (or close to them) may seem somewhat strange (these regions are traditionally associated with cold, which, in turn, is intuitively associated with the absence of solar heat). However, according to the data from various time periods, the averaged value of total solar irradiance in Polar Regions is comparable to European countries like the Netherlands (which produces 22.7% of its electricity from solar energy).[51−55]

4. CONCLUSIONS

In this paper, we present a rational and nontrivial utilization of plasmon-assisted chemistry aimed at CO_2 cycloaddition for the production of technically relevant carbonates at low, down to the arctic, temperatures up to −40 °C. Cycloaddition was implemented under solvent-free conditions by saturating three organic epoxides with CO_2, followed by illumination of dispersed plasmon-active hybrid catalysts by LED at 780 nm. As a hybrid catalyst, we used gold nanoparticles grafted with TBD ligand for spontaneous capture of CO_2 at atmospheric pressure and low temperatures. The plasmon triggering led to the activation of the TBD-CO_2 adduct and its involvement in cycloaddition. Despite the common van't Hoff law, we found that plasmon-induced CO_2 cycloaddition is weakly dependent on the reaction temperature, which in turn allows the use of this reaction even at the temperature of −40 °C. To explain these experimental observations, additional quantum mechanics simulations were performed, which reveal alternative reaction pathways under plasmon triggering, with an activation barrier 3 times lower than in the common case of CO_2 cycloaddition. Low-temperature plasmonic cycloaddition is also facilitated by the enhanced CO_2 solubility in epoxides. Our findings prove that photochemical processes can be carried out in places with sufficient sunlight and low ambient temperatures so that the geography of plasmon chemistry can be expanded significantly. We demonstrated the technological attractiveness of the proposed process in terms of reaction scalability, humidity insensitivity, and the ability of sunlight utilization. We believe that low-temperature plasmonic chemistry can be expanded to other reactions, including carbon dioxide fixation/utilization and dehydrogenation.

■ ASSOCIATED CONTENT

Supporting Information

The Supporting Information is available free of charge at https://pubs.acs.org/doi/10.1021/acscatal.2c05891.

Description of used materials, reagents, and samples preparation methods; measurement and calculation

https://doi.org/10.1021/acscatal.2c05891
ACS Catal. 2023, 13, 3830−3840

techniques; SERS band affiliation; data of organic elemental analysis; schematic representation of the preparation of AuNPs-TBD; AuNPs-TBD, and AuNPs@Al_2O_3-TBD hybrid catalyst characterization: TEM images (including size distribution histograms), Raman, XPS, and UV−vis spectra, DLS results; temperature dependence of CO_2 solubility in epoxides; GC chromatograms, ^{1}H NMR and ^{13}C NMR spectra of produced carbonates; interpretation of ^{1}H NMR and ^{13}C spectra; control experiments: illumination stopping and catalyst leaching, reaction proceeding without TBD grafting, without AuNPs presence or in cyclooctatetraene (triplet state quencher) presence, temperature and plasmon heating controls (including power and light beam radius dependences experiments); demonstration of reaction insensitivity to humidity presence (at low temperature); and DFT-calculated reaction coordinates (PDF)

AUTHOR INFORMATION

Corresponding Author

Oleksiy Lyutakov − *Department of Solid State Engineering, University of Chemistry and Technology, 16628 Prague, Czech Republic; Faculty of Science, J. E. Purkyně University, 40096 Ústí nad Labem, Czech Republic; Institute of Organic Chemistry and Technology, Faculty of Chemical Technology, University of Pardubice, 53210 Pardubice, Czech Republic;* orcid.org/0000-0001-8781-9796; Email: lyutakoo@vscht.cz

Authors

Anna Zabelina − *Department of Solid State Engineering, University of Chemistry and Technology, 16628 Prague, Czech Republic*

Jakub Dedek − *Department of Solid State Engineering, University of Chemistry and Technology, 16628 Prague, Czech Republic*

Olga Guselnikova − *Department of Solid State Engineering, University of Chemistry and Technology, 16628 Prague, Czech Republic*

Denis Zabelin − *Department of Solid State Engineering, University of Chemistry and Technology, 16628 Prague, Czech Republic*

Andrii Trelin − *Department of Solid State Engineering, University of Chemistry and Technology, 16628 Prague, Czech Republic*

Elena Miliutina − *Department of Solid State Engineering, University of Chemistry and Technology, 16628 Prague, Czech Republic*

Zdenka Kolska − *Faculty of Science, J. E. Purkyně University, 40096 Ústí nad Labem, Czech Republic*

Jakub Siegel − *Department of Solid State Engineering, University of Chemistry and Technology, 16628 Prague, Czech Republic*

Vaclav Svorcik − *Department of Solid State Engineering, University of Chemistry and Technology, 16628 Prague, Czech Republic*

Jiri Vana − *Institute of Organic Chemistry and Technology, Faculty of Chemical Technology, University of Pardubice, 53210 Pardubice, Czech Republic*

Complete contact information is available at: https://pubs.acs.org/10.1021/acscatal.2c05891

Notes

The authors declare no competing financial interest.

ACKNOWLEDGMENTS

This work was supported by the GACR under project no. 22-02022S and by UCT Prague and under the project RVO JIGA 126-85-2215.

REFERENCES

(1) Klotzbücher, W. E. Low Temperature Chemistry. In *The Status of Soviet Civil Science: Proceedings of the Symposium on Soviet Scientific Research, NATO Headquarters, Brussels, Belgium, September 24−26, 1986*; Sinclair, C., Ed.; Springer Netherlands: Dordrecht, 1987; pp 211−224 DOI: 10.1007/978-94-009-3647-8_16.

(2) Sekine, Y.; Manabe, R. Reaction Mechanism of Low-Temperature Catalysis by Surface Protonics in an Electric Field. *Faraday Discuss.* **2021**, *229*, 341−358.

(3) Zhang, Z.; Jiang, Z.; Shangguan, W. Low-Temperature Catalysis for VOCs Removal in Technology and Application: A State-of-the-Art Review. *Catal. Today* **2016**, *264*, 270−278.

(4) Razmyar, S.; Sheng, T.; Akter, M.; Zhang, H. Low-Temperature Photocatalytic Hydrogen Addition to Two-Dimensional MoO_3 Nanoflakes from Isopropyl Alcohol for Enhancing Solar Energy Harvesting and Conversion. *ACS Appl. Nano Mater.* **2019**, *2*, 4180−4192.

(5) Silvestre, B. S.; Ţîrcă, D. M. Innovations for Sustainable Development: Moving toward a Sustainable Future. *J. Cleaner Prod.* **2019**, *208*, 325−332.

(6) Ghiat, I.; Al-Ansari, T. A Review of Carbon Capture and Utilisation as a CO_2 Abatement Opportunity within the EWF Nexus. *J. CO_2 Util.* **2021**, *45*, No. 101432.

(7) Report Card. https://arctic.noaa.gov/Report-Card (accessed August 08, 2022).

(8) Li, X.; Yu, J.; Jaroniec, M.; Chen, X. Cocatalysts for selective photoreduction of CO_2 into solar fuels. *Chem. Rev.* **2019**, *119*, 3962−4179.

(9) Birdja, Y. Y.; Pérez-Gallent, E.; Figueiredo, M. C.; Göttle, A. J.; Calle-Vallejo, F.; Koper, M. T. M. Advances and Challenges in Understanding the Electrocatalytic Conversion of Carbon Dioxide to Fuels. *Nat. Energy* **2019**, *4*, 732−745.

(10) Shaikh, R. R.; Pornpraprom, S.; D'Elia, V. Catalytic Strategies for the Cycloaddition of Pure, Diluted, and Waste CO_2 to Epoxides under Ambient Conditions. *ACS Catal.* **2018**, *8*, 419−450.

(11) Linic, S.; Christopher, P.; Ingram, D. B. Plasmonic-Metal Nanostructures for Efficient Conversion of Solar to Chemical Energy. *Nat. Mater.* **2011**, *10*, 911−921.

(12) Wang, W.; Xu, D.; Cheng, B.; Yu, J.; Jiang, C. Hybrid Carbon@TiO_2 Hollow Spheres with Enhanced Photocatalytic CO_2 Reduction Activity. *J. Mater. Chem. A* **2017**, *5*, 5020−5029.

(13) White, J. L.; Baruch, M. F.; Pander, J. E.; Hu, Y.; Fortmeyer, I. C.; Park, J. E.; Zhang, T.; Liao, K.; Gu, J.; Yan, Y.; Shaw, T. W.; Abelev, E.; Bocarsly, A. B. Light-Driven Heterogeneous Reduction of Carbon Dioxide: Photocatalysts and Photoelectrodes. *Chem. Rev.* **2015**, *115*, 12888−12935.

(14) Zhu, Y.; Xu, Z.; Lang, Q.; Jiang, W.; Yin, Q.; Zhong, S.; Bai, S. Grain Boundary Engineered Metal Nanowire Cocatalysts for Enhanced Photocatalytic Reduction of Carbon Dioxide. *Appl. Catal., B* **2017**, *206*, 282−292.

(15) Li, X.; Wen, J.; Low, J.; Fang, Y.; Yu, J. Design and Fabrication of Semiconductor Photocatalyst for Photocatalytic Reduction of CO_2 to Solar Fuel. *Sci. China Mater.* **2014**, *57*, 70−100.

(16) Bai, Y.; Ye, L.; Chen, T.; Wang, P.; Wang, L.; Shi, X.; Wong, P. K. Synthesis of Hierarchical Bismuth-Rich $Bi_4O_5Br_xI_{2-x}$ Solid Solutions for Enhanced Photocatalytic Activities of CO_2 Conversion and Cr(VI) Reduction under Visible Light. *Appl. Catal., B.* **2017**, *203*, 633−640.

(17) Chen, S.; Qi, Y.; Li, C.; Domen, K.; Zhang, F. Surface Strategies for Particulate Photocatalysts toward Artificial Photosynthesis. *Joule* **2018**, *2*, 2260−2288.
(18) Wu, N. Plasmonic Metal−Semiconductor Photocatalysts and Photoelectrochemical Cells: A Review. *Nanoscale* **2018**, *10*, 2679−2696.
(19) DuChene, J. S.; Tagliabue, G.; Welch, A. J.; Cheng, W.-H.; Atwater, H. A. Hot Hole Collection and Photoelectrochemical CO_2 Reduction with Plasmonic Au/p-GaN Photocathodes. *Nano Lett.* **2018**, *18*, 2545−2550.
(20) Li, J.; Ye, Y.; Ye, L.; Su, F.; Ma, Z.; Huang, J.; Xie, H.; Doronkin, D. E.; Zimina, A.; Grunwaldt, J.-D.; Zhou, Y. Sunlight Induced Photo-Thermal Synergistic Catalytic CO_2 Conversion via Localized Surface Plasmon Resonance of MoO_{3-x}. *J. Mater. Chem. A* **2019**, *7*, 2821−2830.
(21) Liu, H.; Dao, T. D.; Liu, L.; Meng, X.; Nagao, T.; Ye, J. Light Assisted CO_2 Reduction with Methane over Group VIII Metals: Universality of Metal Localized Surface Plasmon Resonance in Reactant Activation. *Appl. Catal., B.* **2017**, *209*, 183−189.
(22) Li, S.; Miao, P.; Zhang, Y.; Wu, J.; Zhang, B.; Du, Y.; Han, X.; Sun, J.; Xu, P. Recent Advances in Plasmonic Nanostructures for Enhanced Photocatalysis and Electrocatalysis. *Adv. Mater.* **2021**, *33*, No. 2000086.
(23) Marques Mota, F.; Ha Kim, D. From CO_2 Methanation to Ambitious Long-Chain Hydrocarbons: Alternative Fuels Paving the Path to Sustainability. *Chem. Soc. Rev.* **2019**, *48*, 205−259.
(24) Chai, R.; Liu, Y.; Wang, J.; Liu, Q.; Rui, Z. CO_2 Utilization and Sequestration in Reservoir: Effects and Mechanisms of CO_2 Electrochemical Reduction. *Appl. Energy* **2022**, *323*, No. 119584.
(25) Li, F.; R MacFarlane, D.; Zhang, J. Recent Advances in the Nanoengineering of Electrocatalysts for CO_2 Reduction. *Nanoscale* **2018**, *10*, 6235−6260.
(26) Miliutina, E.; Guselnikova, O.; Soldatova, N. S.; Bainova, P.; Elashnikov, R.; Fitl, P.; Kurten, T.; Yusubov, M. S.; Švorčík, V.; Valiev, R. R.; Chehimi, M. M.; Lyutakov, O.; Postnikov, P. S. Can Plasmon Change Reaction Path? Decomposition of Unsymmetrical Iodonium Salts as an Organic Probe. *J. Phys. Chem. Lett.* **2020**, *11*, 5770−5776.
(27) De Cattelle, A.; Billen, A.; Brullot, W.; Verbiest, T.; Koeckelberghs, G. Plasmonic Heating Using an Easily Recyclable Pd-Functionalized Fe_3O_4/Au Core-Shell Nanoparticle Catalyst for the Suzuki and Sonogashira Reaction. *Appl. Organomet. Chem.* **2020**, *34*, No. e5648.
(28) Guselnikova, O.; Olshtrem, A.; Kalachyova, Y.; Panov, I.; Postnikov, P.; Svorcik, V.; Lyutakov, O. Plasmon Catalysis on Bimetallic Surface—Selective Hydrogenation of Alkynes to Alkanes or Alkenes. *J. Phys. Chem. C* **2018**, *122*, 26613−26622.
(29) Gu, Q.; Jia, Q.; Long, J.; Gao, Z. Heterogeneous Photocatalyzed C−C Cross-Coupling Reactions Under Visible-Light and Near-Infrared Light Irradiation. *ChemCatChem* **2019**, *11*, 669−683.
(30) Guselnikova, O.; Postnikov, P.; Chehimi, M. M.; Kalachyovaa, Y.; Svorcik, V.; Lyutakov, O. Surface Plasmon-Polariton: A Novel Way To Initiate Azide−Alkyne Cycloaddition. *Langmuir* **2019**, *35*, 2023−2032.
(31) Christopher, P.; Xin, H.; Linic, S. Visible-Light-Enhanced Catalytic Oxidation Reactions on Plasmonic Silver Nanostructures. *Nat. Chem.* **2011**, *3*, 467−472.
(32) Zhou, L.; Martirez, J. M. P.; Finzel, J.; Zhang, C.; Swearer, D. F.; Tian, S.; Robatjazi, H.; Lou, M.; Dong, L.; Henderson, L.; Christopher, P.; Carter, E. A.; Nordlander, P.; Halas, N. J. Light-Driven Methane Dry Reforming with Single Atomic Site Antenna-Reactor Plasmonic Photocatalysts. *Nat. Energy* **2020**, *5*, 61−70.
(33) Han, L.; Zhang, L.; Wu, H.; Zu, H.; Cui, P.; Guo, J.; Guo, R.; Ye, J.; Zhu, J.; Zheng, X.; Yang, L.; Zhong, Y.; Liang, S.; Wang, L. Anchoring Pt Single Atoms on Te Nanowires for Plasmon-Enhanced Dehydrogenation of Formic Acid at Room Temperature. *Adv. Sci.* **2019**, *6*, No. 1900006.
(34) Guselnikova, O.; Váňa, J.; Phuong, L. T.; Panov, I.; Rulíšek, L.; Trelin, A.; Postnikov, P.; Švorčík, V.; Andris, E.; Lyutakov, O. Plasmon-Assisted Click Chemistry at Low Temperature: An Inverse Temperature Effect on the Reaction Rate. *Chem. Sci.* **2021**, *12*, 5591−5598.
(35) Guselnikova, O.; Postnikov, P.; Kosina, J.; Kolska, Z.; Trelin, A.; Svorcik, V.; Lyutakov, O. A Breath of Fresh Air for Atmospheric CO_2 Utilisation: A Plasmon-Assisted Preparation of Cyclic Carbonate at Ambient Conditions. *J. Mater. Chem. A* **2021**, *9*, 8462−8469.
(36) Obryk, M. K.; Fountain, A. G.; Doran, P. T.; Lyons, W. B.; Eastman, R. Drivers of Solar Radiation Variability in the McMurdo Dry Valleys, Antarctica. *Sci. Rep.* **2018**, *8*, No. 5002.
(37) Stanek, W.; Valero, A.; Calvo, G.; Czarnowska, L. Resources. Production. Depletion. In *Thermodynamics for Sustainable Management of Natural Resources. Green Energy and Technology*; Stanek, W., Ed.; Springer International Publishing: Cham, 2017; pp 7−36.
(38) Dawson, I. G. J.; Johnson, J. E. V. Does Size Matter? A Study of Risk Perceptions of Global Population Growth. *Risk Anal.* **2017**, *37*, 65−81.
(39) Perez, R.; Lorenz, E.; Pelland, S.; Beauharnois, M.; Van Knowe, G.; Hemker, K.; Heinemann, D.; Remund, J.; Müller, S. C.; Traunmüller, W.; Steinmauer, G.; Pozo, D.; Ruiz-Arias, J. A.; Lara-Fanego, V.; Ramirez-Santigosa, L.; Gaston-Romero, M.; Pomares, L. M. Comparison of Numerical Weather Prediction Solar Irradiance Forecasts in the US, Canada and Europe. *Sol. Energy* **2013**, *94*, 305−326.
(40) Ezendam, S.; Herran, M.; Nan, L.; Gruber, C.; Kang, Y.; Gröbmeyer, F.; Lin, R.; Gargiulo, J.; Sousa-Castillo, A.; Cortés, E. Hybrid Plasmonic Nanomaterials for Hydrogen Generation and Carbon Dioxide Reduction. *ACS Energy Lett.* **2022**, *7*, 778−815.
(41) Linic, S.; Chavez, S.; Elias, R. Flow and Extraction of Energy and Charge Carriers in Hybrid Plasmonic Nanostructures. *Nat. Mater.* **2021**, *20*, 916−924.
(42) Villiers, C.; Dognon, J.-P.; Pollet, R.; Thuéry, P.; Ephritikhine, M. An Isolated CO_2 Adduct of a Nitrogen Base: Crystal and Electronic Structures. *Angew. Chem., Int. Ed.* **2010**, *49*, 3465−3468.
(43) Foerster, B.; Spata, V. A.; Carter, E. A.; Sönnichsen, C.; Link, S. Plasmon Damping Depends on the Chemical Nature of the Nanoparticle Interface. *Sci. Adv.* **2019**, *5*, No. eaav0704.
(44) Chavez, S.; Aslam, U.; Linic, S. Design Principles for Directing Energy and Energetic Charge Flow in Multicomponent Plasmonic Nanostructures. *ACS Energy Lett.* **2018**, *3*, 1590−1596.
(45) Décultot, M.; Ledoux, A.; Fournier-Salaün, M.-C.; Estel, L. Solubility of CO_2 in Methanol, Ethanol, 1,2-Propanediol and Glycerol from 283.15 K to 373.15 K and up to 6.0 MPa. *J. Chem. Thermodyn.* **2019**, *138*, 67−77.
(46) Baffou, G.; Bordacchini, I.; Baldi, A.; Quidant, R. Simple Experimental Procedures to Distinguish Photothermal from Hot-Carrier Processes in Plasmonics. *Light Sci. Appl.* **2020**, *9*, No. 108.
(47) Boerigter, C.; Campana, R.; Morabito, M.; Linic, S. Evidence and Implications of Direct Charge Excitation as the Dominant Mechanism in Plasmon-Mediated Photocatalysis. *Nat. Commun.* **2016**, *7*, No. 10545.
(48) Linic, S.; Aslam, U.; Boerigter, C.; Morabito, M. Photochemical Transformations on Plasmonic Metal Nanoparticles. *Nat. Mater.* **2015**, *14*, 567−576.
(49) Kale, M. J.; Avanesian, T.; Xin, H.; Yan, J.; Christopher, P. Controlling Catalytic Selectivity on Metal Nanoparticles by Direct Photoexcitation of Adsorbate−Metal Bonds. *Nano Lett.* **2014**, *14*, 5405−5412.
(50) Ma, J.; Zhang, X.; Zhao, N.; Al-Arifi, A. S. N.; Aouak, T.; Al-Othman, Z. A.; Xiao, F.; Wei, W.; Sun, Y. Theoretical Study of TBD-Catalyzed Carboxylation of Propylene Glycol with CO_2. *J. Mol. Catal. A: Chem.* **2010**, *315*, 76−81.
(51) Schmutz, W. K. Changes in the Total Solar Irradiance and Climatic Effects. *J. Space Weather Space Clim.* **2021**, *11*, No. 40.
(52) Van Heerwaarden, C. C.; Mol, W. B.; Veerman, M. A.; Benedict, I.; Heusinkveld, B. G.; Knap, W. H.; Kazadzis, S.; Kouremeti, N.; Fiedler, S. Record High Solar Irradiance in Western Europe during First COVID-19 Lockdown Largely Due to Unusual Weather. *Commun. Earth Environ.* **2021**, *2*, No. 37.

https://doi.org/10.1021/acscatal.2c05891
ACS Catal. 2023, 13, 3830−3840

(53) Here's how solar energy saved Europeans $29 billion this summer. World Economic Forum. https://www.weforum.org/agenda/2022/10/solar-power-europe-energy-transition/ (accessed Jan 05, 2023).
(54) Przybylak, R.; Svyashchennikov, P. N.; Uscka-Kowalkowska, J.; Wyszyński, P. Solar Radiation in the Arctic during the Early Twentieth-Century Warming (1921−50): Presenting a Compilation of Newly Available Data. *J. Clim.* **2021**, *34*, 21−37.
(55) Brun, P.; Zimmermann, N. E.; Hari, C.; Pellissier, L.; Karger, D. N. Global Climate-Related Predictors at Kilometer Resolution for the Past and Future. *Earth Syst. Sci. Data* **2022**, *14*, 5573−5603.

https://doi.org/10.1021/acscatal.2c05891
ACS Catal. 2023, 13, 3830−3840